DOI: 10.1002/chem.201102632

Pt–Cu and Pt–Pd–Cu Concave Nanocubes with High-Index Facets and Superior Electrocatalytic Activity

An-Xiang Yin, Xiao-Quan Min, Wei Zhu, Wen-Chi Liu, Ya-Wen Zhang,* and Chun-Hua Yan*[a]

High-index-facets-enclosed (HIFs-enclosed) nanocrystals (such as metals[1] and metal oxides[2]) have drawn great interests both theoretically and technologically. Such nanocrystals have shown significantly enhanced catalytic activity in many reactions because of the existence of high density atomic steps, ledges and kinks on the HIFs (as compared to those common basal facets, e.g., {100}, {111}, and {110}).[3] So far, there are several reports on the electrochemical or solution-chemical synthesis of monometallic nanocrystals with HIFs (e.g., tetrahexahedral (THH) and trioctahedral (TOH) Pt nanocrystals,[1] concave Pt nanocubes[4] and polyhedrons,[5] TOH Au nanocrystals,[6a,b] THH Au nanocrystals,[6c] and Au concave nanocubes,[7]). However, there are still few works on the synthesis of multimetallic nanocrystals with HIFs (e.g., THH and TOH Pd@Au nanocrystals,[8] Pt@Pd concave nanostructures[9]). It is still challenging to obtain the active but thermodynamically unfavorable HIFs in solution synthesis. Recent researches indicate that the exposing and stabilizing of HIFs could be realized by the tuning of growth kinetics,[1,4] the selective adsorption of certain chemical species,[5–7] and the epitaxial growth from HIFs enclosed seeds.[8]

Pt-based nanocrystals are the most promising catalysts for wide applications in oil refinement, fine chemicals, and fuel cells. More recently, it has been demonstrated that the catalytic activity of Pt-based nanocatalysts can be considerably enhanced by tuning their electronic structures with the formation of bimetallic structures.[10] Several Pt–M (M = Fe, Co, Ni, Cu, Mn, Ru, Au, Pd) nanocrystals with high electrocatalytic activity have been obtained through the co-reduction method or seeded growth protocols.[11] Among them, Pt–Cu nanocrystals resulted promising catalysts in methanol, formic acid electro-oxidation, and oxygen reduction reactions. For example, Pt–Cu nanocubes (NCs) showed better catalytic activity toward methanol and formic acid electro-oxidations than Pt nanocrystals.[11d,i] Surface dealloyed Pt–Cu nanostructures[12] and Pt monolayer on porous Pd–Cu alloy nanoparticles[13] showed better activity to oxygen reduction reactions. The activity enhancement for these Pt–Cu nanostructures could be ascribed to the modulation of surface electronic structures via the tuning of the internal lattice strains of the nanostructures.[14] However, up to date, researches on the synthesis and electrocatalytic behaviors of Pt-based alloy nanostructures with HIFs are still insufficient.

Herein, we present a highly-selective synthesis of Pt–Cu and Pt–Pd–Cu concave nanocubes (CNCs) enclosed by the {*hk*0} HIFs through progressive galvanic replacements in a one-pot hydrothermal process. The as-prepared bimetallic or trimetallic CNCs showed superior electrocatalytic activity to Pt NCs and commercial Pt/C catalyst for methanol oxidations.

Monodisperse Pt–Cu NCs and Pt–Cu CNCs could be selectively prepared through the co-reduction of Pt^{II} and Cu^{II} species by poly(vinylpyrrolidone) (PVP) molecules in aqueous solutions with different amounts of Br^- and H^+ ions (for detailed synthesis parameters, please see the Experimental Section and the Supporting Information). Single-crystalline Pt–Cu NCs ((7.0 ± 0.7) nm; with a shape selectivity of 93%) were bounded by six {100} facets (Figure 1a and b and Figure S1a in the Supporting Information). Single-crystalline Pt–Cu CNCs ((11.2 ± 1.5) nm; with a shape selectivity of 89%) were enclosed by several concave facets or steps (Figure 1d–f and Figure S1c and e). Figure S1f shows the image of a single Pt–Cu CNC projected along the [111] axis. Figure 1e and f show the high-resolution transmission electron microscopy (HRTEM) images of a Pt–Cu CNC. Figure 1g is the corresponding fast Fourier transform (FFT) pattern of the HRTEM image in Figure 1e. As confirmed by the FFT pattern (Figure 1g), the HRTEM image (Figure 1e) was projected along the [100] axis. Angles between several concave facets or steps projected on the *X*–*Y* plane and the {100} facets of an ideal cube, as shown in Figure 1e, were 10°, 19°, 33°, and 36°, thus suggesting that there would be several high-index {*hk*0} facets or steps instead of the three basal facets ({100}, {110}, and {111}), if considering the present alloy CNCs have the same *fcc* structure as pure Pt.[4]

[a] A.-X. Yin, X.-Q. Min, W. Zhu, W.-C. Liu, Prof. Dr. Y.-W. Zhang, Prof. Dr. C.-H. Yan
Beijing National Laboratory for Molecular Sciences
State Key Laboratory of Rare Earth
Materials Chemistry and Applications
PKU-HKU Joint Laboratory in
Rare Earth Materials and Bioinorganic Chemistry
College of Chemistry and Molecular Engineering
Peking University, Beijing, 100871 (P. R. China)
Fax: (+86) 10-6275-4179
E-mail: ywzhang@pku.edu.cn
yan@pku.edu.cn

Supporting information for this article is available on the WWW under http://dx.doi.org/10.1002/chem.201102632.

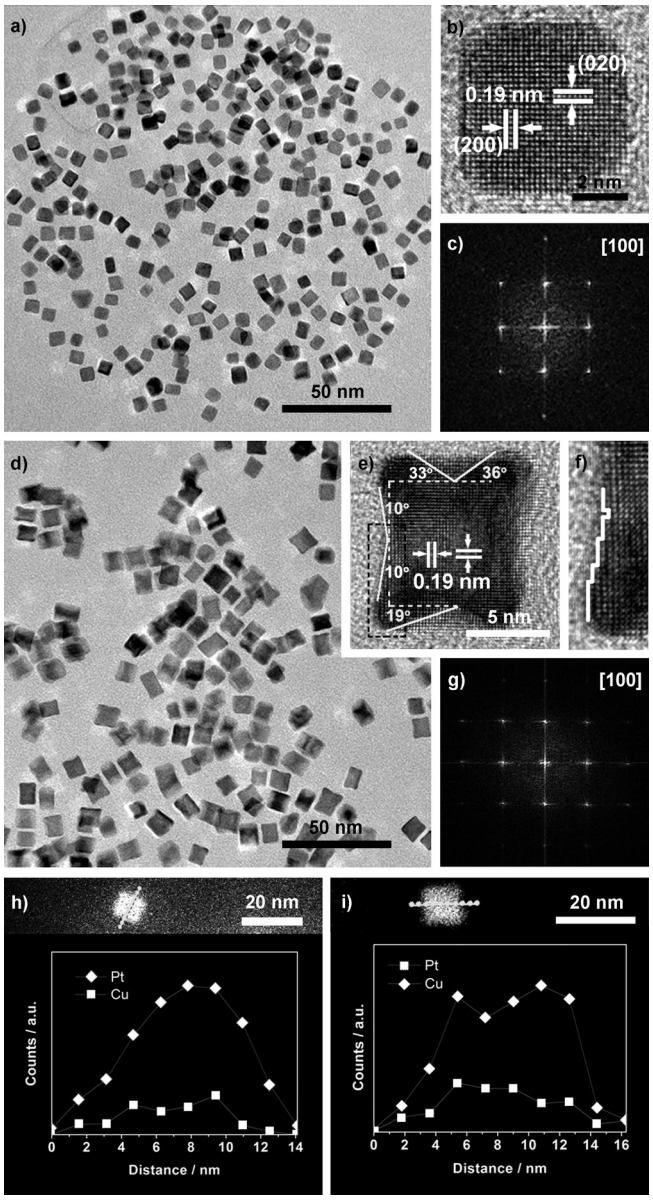

Figure 1. a–c) TEM and HRTEM images, FFT patterns of Pt–Cu NCs and d–g) CNCs. Single-particle STEM-EDS line-scan profiles of h) Pt–Cu NCs and i) CNCs. Panel f is the magnified HRTEM image taken from the same CNC in panel e. Panel c and g are the corresponding FFT patterns of the HRTEM images in panel b and e, respectively.

The magnified HRTEM image further showed the concave high-index steps (Figure 1 f). In addition, the observation of large amounts of Pt–Cu CNCs revealed that most of these concave HIFs are of the mixture of several {*hk*0} facets or steps other than a specific high-index crystal plane. Molar ratios of Pt/Cu in the Pt–Cu NCs and CNCs were monitored with both inductively coupled plasma-atomic emission spectrometry (ICP-AES) analysis (Pt/Cu = 88:12 and 89:11 for Pt–Cu NCs and CNCs, respectively) and energy dispersive X-ray spectroscopy (EDS) (Pt/Cu = 89:11 for both Pt–Cu NCs and CNCs) (Figure S1 b and d and Table S1), although the molar ratios of Pt/Cu calculated from the Pt^{II} and Cu^{II} precursors were 1:1. The reason for that less amounts of Cu^{II} species than Pt^{II} ones were reduced by PVP can be ascribed to the lower reduction potential of Cu^{II} species than that of the Pt^{II} ones. The molar fraction of Cu in these as-prepared NCs or CNCs could be increased when a larger amount of $CuCl_2$ sources were employed in the synthesis. However, a shape variation of these nanocrystals would also be observed simultaneously when the amount of copper precursors was increased, as discussed below.

Further characterizations of the Pt–Cu bimetallic NCs and CNCs were carried out and presented in the Supporting Information. X-ray diffraction (XRD) patterns of Pt–Cu NCs and CNCs confirmed that they were in *fcc* structures with the diffraction peaks slightly shifted to higher angles as compared to standard Pt data, suggesting the smaller crystal parameters due to the alloying of Pt atoms with smaller Cu atoms (Figure S2). High angle annular dark field-scanning transmission electron microscopy (HAADF-STEM) images (Figure S3) demonstrated the cubic or concave morphologies of the Pt-Cu NCs or CNCs, respectively (Figure S3). Single-particle STEM-EDS line-scan profiles (Figure 1 h and i) showed that the distributions of Pt and Cu in the nanocrystals were in well agreement with their cubic or concave shapes without obvious core-shell structures.

A series of control experiments were carried out to reveal the possible growth mechanism of these Pt–Cu CNCs. First, roles of the Cu^{2+}, H^+ and Cl^- species in the forming of CNCs were examined. As shown in Figure S4 and S5, no CNCs could be obtained without the addition of Cu^{2+} precursors or HCl solutions (the increasing of Cu^{2+} precursor concentration would lead to the forming of Pt–Cu CNCs even at high pH values, as discussed below).The substitution of HCl solutions with HBr solutions had no significant effects in the shape-evolution of these nanocrystals (Figure S6), suggesting that the Cl^- mediated etching process might not play a critical role on the formation of Pt–Cu concave structures. Second, the effects of different concentrations of Cu^{2+}, H^+, and Br^- precursors ($c(Cu^{2+})$, $c(H^+)$ and $c(Br^-)$, respectively) on the shape evolution of Pt–Cu nanocrystals were investigated. When the $c(Cu^{2+})$ was increased to 3 times of the Pt^{II} precursor (0.090 mmol of $CuCl_2$ and 0.030 mmol of K_2PtCl_4), Pt–Cu CNCs instead of NCs could be obtained (Figure S7 a and b) (Pt/Cu ≈ 3:1 in the obtained CNCs, as revealed by EDS spectrum). When the $c(Cu^{2+})$ was decreased to 1/3 of the Pt^{II} precursors (0.010 mmol of $CuCl_2$ and 0.030 mmol of K_2PtCl_4), no Pt–Cu CNCs but Pt–Cu NCs could be obtained with the other reaction parameters unchanged (Figure S7 c and d) (Pt/Cu ≈ 16:1 in the prepared NCs, as revealed by EDS spectrum). The effects of different $c(H^+)$ and $c(Br^-)$ were shown in Figure S8: When the amounts of KBr used were increased from 1.5 mmol to 9.0 mmol, more regular NCs would be formed at high pH values (Figure S8 a–d and e–h) and CNCs would be obtained at low pH values (Figure S8 i–l, m–p and q–t). When the amounts of HCl employed were increased from 0 to 0.90 mmol, the shapes of as-prepared Pt-Cu nanocrystals would change from polyhedrons to irregular concave nano-

crystals at low $c(Br^-)$ (Figure S8 a,e,i,m,q), or change from NCs to CNCs at high $c(Br^-)$ (Figure S8 d,h,l,p,t). In short, the increasing of the concentrations of Cu^{2+}, H^+, or Br^- precursors would promote the forming of Pt–Cu CNCs. With the increase of Cu^{2+} concentrations, more CNCs could be obtained with the simultaneous increase of the molar fractions of Cu in these CNCs. With larger amount of HCl and KBr employed in synthesis, more uniform CNCs could be obtained. However, the use of large amounts of H^+ and Br^-would lead to the increasing of particle sizes and the aggregations of the Pt–Cu CNCs (Figure S8 t).

Time sequential evolution experiments revealed the progressive procedure for the forming of Pt–Cu CNCs during the hydrothermal process. In the first 4 h, the Pt–Cu nanocrystals gradually grew from sphere-like nanopolyhedrons (Figure S9 a) into NCs (Figure S9 b) and then into CNCs (Figure S9 c and d). After that, the concave structures were well maintained in the next 2 h (Figure S9 e).

Based on these experimental facts, we suggest a plausible mechanism in which galvanic replacement may play an important role for the synthesis of these Pt–Cu bimetallic CNCs, as shown in Scheme 1. The precursors, Pt^{II} and Cu^{II}

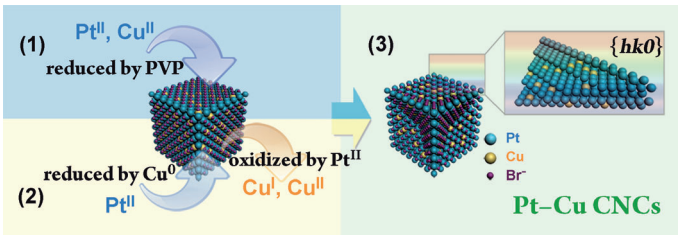

Scheme 1. Progressive formation of Pt–Cu CNCs.

species, as well as the imported Br^- and H^+ species, would play key roles in the forming of CNCs in the hydrothermal process. On the one hand, the abundant of Br^- species in solution would significantly alter the reaction kinetics since the reduction potential of $[PtBr_4]^{2-}$ species were much lower than the $[PtCl_4]^{2-}$ species from the K_2PtCl_4 precursors.[9] And a much slower reducing rate would help the forming of concave nanocrystals, as revealed by Xia and co-workers in the synthesis of Pt CNCs.[4] On the other hand, as observed in the time sequential TEM images (Figure S9), the forming of Pt–Cu CNCs could be briefly divided into two steps. First, once the seeds were formed in the hot solution, galvanic reactions between the oxidative Pt^{II} and Cu^{II} species and the reductive PVP molecules would occur at the surfaces of these metal seeds. As a result, these seeds would then grow bigger into nanopolyhedrons of irregular shapes and NCs (Figure S9 a and b) with the selective adsorption of Br^- on the {100} facets. Second, as similar to the galvanic replacements between Pd and Pt species,[9] the galvanic replacements between the surface reductive Cu(0) atoms of the as-formed NCs and the oxidative species in solutions ($[PtBr_4]^{2-}$, H^+) would take place. Due to the selective adsorption of Br^- on the {100} facets of these Pt–Cu NCs, the $[PtBr_4]^{2-}$ species might have a higher concentration near these {100} facets.[9] As a result, the Cu atoms on the {100} facets would be preferentially oxidized by these $[PtBr_4]^{2-}$ complex and then dissolved into the solution. Meanwhile, the electrons produced by the oxidation of Cu atoms would migrate quickly in the whole Pt–Cu nanocrystals and then reduce the oxidative Pt^{II}/Cu^{II} species into Pt/Cu atoms, which would subsequently deposit at the corners or edges of these NCs initially evolved from the particles of irregular polyhedrons, and finally lead to the forming of the concave high-index steps (a mixture of several {*hk*0} facets) on these CNCs (Figure S9 c and d) with surface-adsorbed Br^- species (Figure S10).[9]

This strategy for preparing Pt–Cu CNCs could be extended to the synthesis of Pt–Pd–Cu trimetallic CNCs. As shown in Figure 2 and Figure S11, with the addition of certain amount of Na_2PdCl_4 as Pd^{II} precursors, two kinds of trimetallic CNCs, denoted as Pt–Pd–Cu CNCs-1 (17.3 ± 2.9 nm; with a shape selectivity of 96 %; Pt/Pd/Cu = 42:46:12 by ICP-AES or 45:43:12 by EDS; Figure 2 and Figure S11 a and b) and Pt–Pd–Cu CNCs-2 (15.4 ± 2.5 nm; with a shape selectivity of 87 %; Pt/Pd/Cu = 62:22:16 by ICP-AES or 63:22:15 by EDS; Figure S11 c and d), could be obtained. These trimetallic CNCs were bounded with several high-index steps, as indicated by the HRTEM images (Figure 2 b

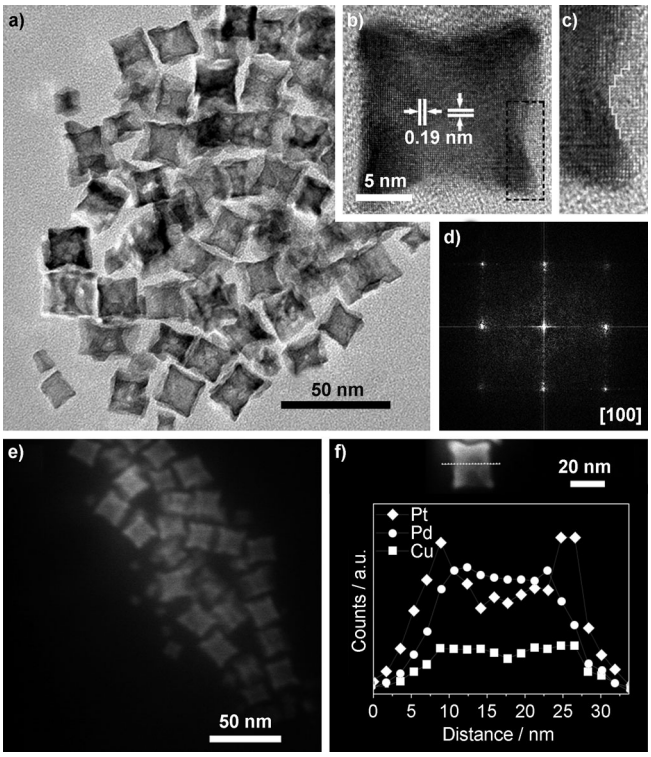

Figure 2. a) TEM and b,c) HRTEM images, d) FFT pattern, e) HAADF-STEM images, and f) single-particle STEM-EDS line-scan profile of Pt–Pd–Cu CNCs. Panel c is the magnified HRTEM image taken from the same CNC in panel b. Panel d is the corresponding FFT pattern of the HRTEM image in panel b.

and c and Figure S11c). XRD patterns of these Pt–Pd–Cu CNCs also reflected the *fcc* structures with the diffraction peaks shifted to higher angles as compared to standard Pt or Pd data (Figure S2). HAADF-STEM images (Figure 2e and Figure S12a) also confirmed the concave structure of these CNCs. Single-particle STEM-EDS line-scan profiles (Figure 2f and Figure S12b) indicated that the distributions of Pt, Pd, and Cu atoms were in well accordance to the concave shape of these trimetallic CNCs and no obvious core-shell structures were observed. In addition, we also tried the preparation of Pd–Cu nanocrystals through the similar protocols. However, no CNCs but only multi-twinned nanocrystals could be obtained (Figure S13), as similar to the findings of Huang and coworkers.[15]

To examine the composition and shape effects on the catalytic activities of these nanocrystals, electro-oxidations of methanol on Pt–Cu NCs, Pt–Cu CNCs, Pt–Pd–Cu CNCs-1, Pt–Pd–Cu CNCs-2, Pt NCs and commercial Pt/C catalysts (Figure S14) were carried out with a N_2 protected three-electrode system. Before each electrochemical test, 4 h of room temperature UV/Ozone treatment was used to remove the capping agents (PVP, for example) covered on the nanocrystal surfaces.[11f,16] As shown in Figure S15, the shape, size and distributions of Pt–Cu CNCs were well maintained even after 12 h of the UV/Ozone treatment. Thus, this non-destructive UV/Ozone treatment could be widely used in the pre-treatment of nanocatalysts capped by organic molecules.[16]

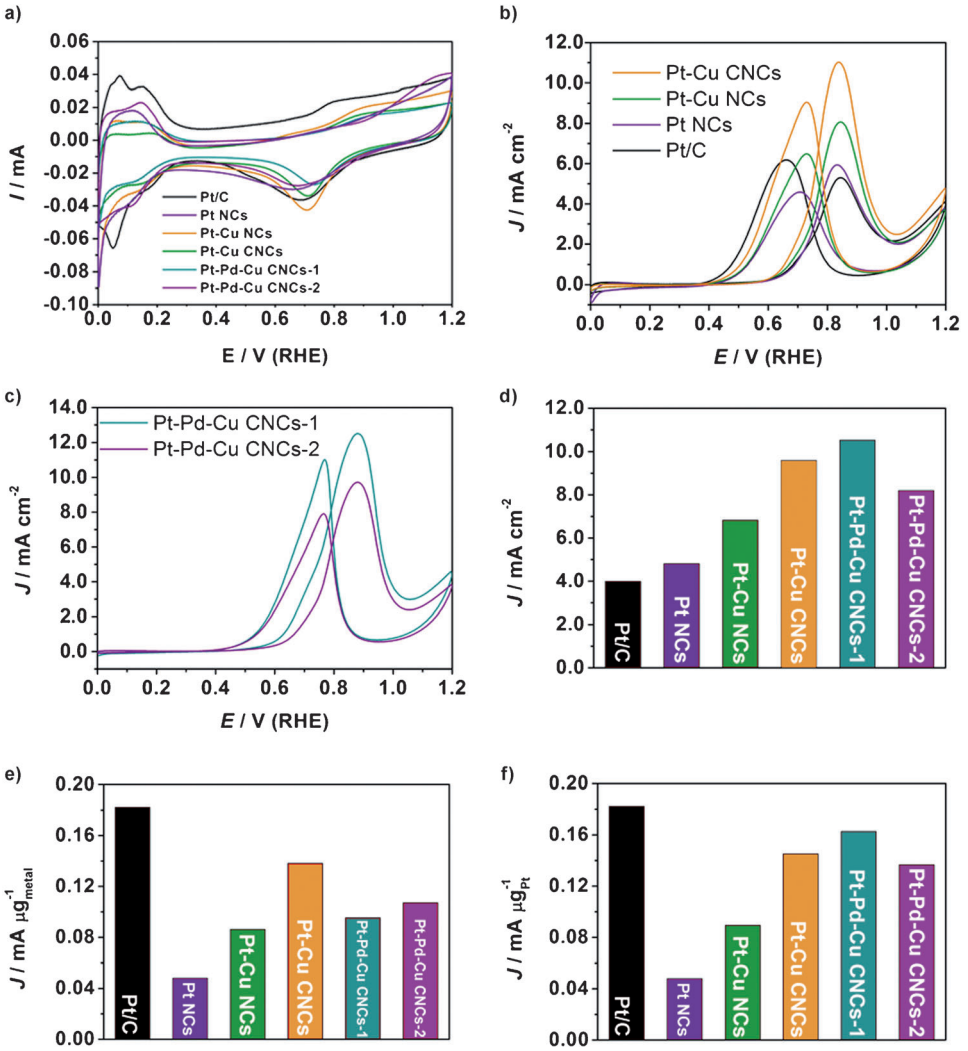

Figure 3. Cyclic voltammetry (CV, scan rate: 50 mVs^{-1}) curves of Pt/C, Pt NCs, Pt–Cu NCs, Pt–Cu CNCs, Pt–Pd–Cu CNCs-1, and Pt–Pd–Cu CNCs-2 in a) $HClO_4$ (0.1 M) and b,c) $HClO_4$ (0.1 M) + CH_3OH (1 M). d) Specific activity and e,f) mass activity for methanol oxidation on these six different kinds of catalysts. In panel e and f, the current density was normalized in reference to the unit weight of total metal and Pt loaded on the working electrode, respectively.

Steady cyclic voltammetry (CV) curves (after 10 cycles of CV sweeps from 0 to 1.2 V (vs. RHE) at the scan rate of 100 $mV s^{-1}$) of H-ad/desorption on these Pt–Cu NCs and CNCs in 0.1 M $HClO_4$ solutions (Figure 3a) shows obvious H-ad/desorption peaks and no Cu stripping peaks, revealing that there were few Cu atoms at the surface of nanocrystals although the surface energy of Cu is lower.[12] In addition, the XPS results also suggested a possible Pt-rich skin of these nanocrystals (Table S1). However, the bulk chemical compositions of the present nanocatalysts changed little before and after electrochemical measurements, as demonstrated by ICP-AES analysis (Table S1). Therefore, the forming of these Cu-poor "skins" of the NCs and CNCs could be ascribed to the surface dealloying process of these bimetallic or trimetallic nanocrystals caused by the galvanic replacements between Pt and Cu species in the hydrothermal synthesis, as revealed by the data of surface components determined by XPS method (Table S1).

As shown in Figure 3b–d and Figure S16, the as-prepared Pt–Cu NCs, CNCs, Pt–Pd–Cu CNCs-1 and CNCs-2 nanocrystals exhibited higher activities than Pt NCs for methanol oxidation, while the activity stability of all the nanocatalysts was comparable with Pt/C. The Pt–Cu NCs showed higher specific activity than Pt NCs and commercial Pt/C catalysts, and the Pt–Cu CNCs showed even higher specific activity than the Pt–Cu NCs, although the bulk and surface compo-

sitions of both of them are similar as revealed by EDS and ICP-AES analyses (Table S1). In addition, both the Pt–Pd–Cu CNCs-1 and CNCs-2 nanocrystals showed higher specific activities than Pt NCs and commercial Pt/C catalysts, with the Pt–Pd–Cu CNCs-1 catalysts a little more active than the CNCs-2, as shown in Figure 3c,d. These four kinds of alloy nanocrystals also showed higher mass activity than as-prepared Pt NCs, while the commercial Pt/C catalyst showed the highest mass activity than all of the as-prepared nanocrystals (Figure 3e and f) due to their ultra-small particle sizes (<3 nm) and large surface areas. The Pt–Pd–Cu CNCs-1 and CNCs-2 exhibited lower mass activity (per unit weight of total metal) than the Pt–Cu CNCs because of their much bigger size.

The enhancement in electrochemical activity for these Pt-based bimetallic or trimetallic NCs and CNCs could be the result of both the composition and shape effects. First, the enhancement of the catalytic activity of Pt–Cu NCs as compared with Pt NCs could be ascribed to the composition effect.[11d,i] The alloying with other metal elements (e.g., Cu and Pd) would modulate the surface electronic structures of Pt-based nanocrystals and thus promote the catalytic activities.[10,12,14] Second, the further activity enhancement of Pt–Cu CNCs was due to the exposing of highly active HIFs in these CNCs.[1,4] These HIFs would provide much more active sites as atomic steps, ledges and kinks at the surface of these CNCs and thus enhance the catalytic activities.[3]

In summary, we have obtained Pt–Cu bimetallic NCs, CNCs, and Pt–Pd–Cu trimetallic CNCs with variable compositions through the fine control of the reaction kinetics and the galvanic replacement process in the one-pot hydrothermal synthesis. The CNCs were enclosed by several concave {*hk*0} high-index steps and facets. After UV/Ozone cleaning, these CNCs showed much higher specific activity than Pt NCs and commercial Pt/C catalysts in methanol oxidations. The modifications of both the surface electronic structures (the alloying of Pt with Cu and Pd) and the surface atomic arrangements (the exposing of HIFs) have been demonstrated as an effective way to enhance the catalytic performances of Pt-based nanocrystals.

Experimental Section

Synthesis of Pt–Cu NCs: In a typical synthesis of Pt–Cu NCs, K_2PtCl_4 (0.030 mmol), $CuCl_2$ (0.030 mmol), KBr (9 mmol), and PVP (100 mg) were dissolved in water. Then, 0.15 mL of 1 M HCl solution was added in the mixture solution and the total volume was adjusted to 15 mL. The homogeneous yellow–brown solution was transferred to a 25 mL Teflon-lined stainless steel autoclave and sealed. The autoclave was then heated at 160 °C for 4 h before it was cooled down to room temperature. The black nanocrystal dispersions were then centrifuged, collected, and washed.

Synthesis of Pt–Cu CNCs: The synthesis of Pt–Cu CNCs was similar to the synthesis of Pt–Cu NCs except that the amount of 1 M HCl solutions was increased to 0.30 mL. Moreover, Pt–Cu CNCs could be prepared with various amounts of HCl and KBr, as detailed in Figure S8.

Synthesis of Pt–Pd–Cu CNCs-1: The synthesis of Pt–Pd–Cu CNCs-1 was similar to the synthesis of Pt–Cu CNCs except that 0.030 mmol of Na_2PdCl_4 was added into the starting solution, the amount of $CuCl_2$ was doubled to 0.060 mmol and the amount of 1 M HCl solutions was kept at 0.050 mL.

Synthesis of Pt–Pd–Cu CNCs-2: The synthesis of Pt–Pd–Cu CNS-2 nanocrystals was similar to that of Pt–Pd–Cu CNS-1, except that the amount of K_2PtCl_4 and Na_2PdCl_4 was adjusted to 0.045 and 0.015 mmol, respectively.

Electrochemical measurements: Electrochemical measurements were carried out with a CHI 840B electrochemical analyzer (CH Instrument, TX, USA). A three-electrode cell was used with a glassy carbon (GC) electrode (6 mm in diameter) as the work electrode, a AgCl/Ag/KCl (saturated) electrode as the reference electrode and a Pt wire as the counter electrode. For more details on the synthesis, instrumentation and electrocatalytic measurements of the obtained nanocrystals, please see the experiment section in the Supporting Information.

Acknowledgements

This work was financially supported by the NSFC (Grant Nos. 21025101, 20871006, and 20821091). Y. W. Z. particularly appreciates the financial aid of China National Funds of Distinguished Young Scientists from the NSFC.

Keywords: concave nanocubes · electrocatalysis · high-index facets · nanostructures · platinum

[1] N. Tian, Z. Y. Zhou, S. G. Sun, Y. Ding, Z. L. Wang, *Science* **2007**, *316*, 732.
[2] a) M. Leng, M. Z. Liu, Y. B. Zhang, Z. Q. Wang, C. Yu, X. G. Yang, H. J. Zhang, C. Wang, *J. Am. Chem. Soc.* **2010**, *132*, 17084; b) H. B. Jiang, Q. Cuan, C. Z. Wen, J. Xing, D. Wu, X. Q. Gong, C. Z. Li, H. G. Yang, *Angew. Chem.* **2011**, *123*, 3848; *Angew. Chem. Int. Ed.* **2011**, *50*, 3764.
[3] G. A. Somorjai, D. W. Blakely, *Nature* **1975**, *258*, 580.
[4] T. Yu, D. Y. Kim, H. Zhang, Y. N. Xia, *Angew. Chem.* **2011**, *123*, 2825; *Angew. Chem. Int. Ed.* **2011**, *50*, 2773.
[5] X. Q. Huang, Z. P. Zhao, J. M. Fan, Y. M. Tan, N. F. Zheng, *J. Am. Chem. Soc.* **2011**, *133*, 4718.
[6] a) Y. Y. Ma, Q Kuang, Z. Y. Jiang, Z. X. Xie, R. R. Huang, L. S. Zheng, *Angew. Chem.* **2008**, *120*, 9033; *Angew. Chem. Int. Ed.* **2008**, *47*, 8901; b) H. L. Wu, C. H. Kuo, M. H. Huang, *Langmuir* **2010**, *26*, 12307; c) T. Ming, W. Feng, Q. Tang, F. Wang, L. D. Sun, J. F. Wang, C. H. Yan, *J. Am. Chem. Soc.* **2009**, *131*, 16350.
[7] J. A. Zhang, M. R. Langille, M. L. Personick, K. Zhang, S. Y. Li, C. A. Mirkin, *J. Am. Chem. Soc.* **2010**, *132*, 14012.
[8] a) C. L. Lu, K. S. Prasad, H. L. Wu, J. A. Ho, M. H. Huang, *J. Am. Chem. Soc.* **2010**, *132*, 14546; b) Y. Yu, Q. B. Zhang, B. Liu, J. Y. Lee, *J. Am. Chem. Soc.* **2010**, *132*, 18258; c) F. Wang, C. H. Li, L. D. Sun, H. S. Wu, T. Ming, J. F. Wang, J. C. Yu, C. H. Yan, *J. Am. Chem. Soc.* **2011**, *133*, 1106.
[9] H. Zhang, M. S. Jin, J. G. Wang, W. Y. Li, P. H. C. Camargo, M. J. Kim, D. R. Yang, Z. X. Xie. Y. N. Xia, *J. Am. Chem. Soc.* **2011**, *133*, 6078.
[10] a) S. Alayoglu, A. U. Nilekar, M. Mavrikakis, B. Eichhorn, *Nat. Mater.* **2008**, *7*, 333; b) A. U. Nilekar, S. Alayoglu, B. Eichhorn, M. Mavrikakis, *J. Am. Chem. Soc.* **2010**, *132*, 7418.
[11] a) V. R. Stamenkovic, B. S. Mun, M. Arenz, K. J. J. Mayrhofer, C. A. Lucas, G. F. Wang, P. N. Ross, N. M. Markovic, *Nat. Mater.* **2007**, *6*, 241; b) H. Lee, S. E. Habas, G. A. Somorjai, P. D. Yang, *J. Am. Chem. Soc.* **2008**, *130*, 5406; c) B. Lim, M. J. Jiang, P. H. C. Camargo, E. C. Cho, J. Tao, X. M. Lu, Y. M. Zhu, Y. N. Xia, *Science* **2009**, *324*, 1302; d) D. Xu, Z. P. Liu, H. Z. Yang, Q. S. Liu, J. Zhang, J. Y. Fang, S. Z. Zou, K. Sun, *Angew. Chem.* **2009**, *121*, 4281; *Angew. Chem. Int. Ed.* **2009**, *48*, 4217; e) J. Zhang, J. Y. Fang, *J. Am. Chem. Soc.* **2009**,

131, 18543; f) Y. J. Kang, C. B. Murray, *J. Am. Chem. Soc.* **2010**, *132*, 7568; g) J. Kim, Y. Lee, S. H. Sun, *J. Am. Chem. Soc.* **2010**, *132*, 4996; h) D. S. Wang, Q. Peng, Y. D. Li, *Nano Res.* **2010**, *3*, 574; i) D. Xu, S. Bliznakov, Z. P. Liu, J. Y. Fang, N. Dimitrov, *Angew. Chem.* **2010**, *122*, 1304; *Angew. Chem. Int. Ed.* **2010**, *49*, 1282; j) H. Z. Yang, J. Zhang, K. Sun, S. Z. Zou, J. Y. Fang, *Angew. Chem.* **2010**, *122*, 7000; *Angew. Chem. Int. Ed.* **2010**, *49*, 6848; k) J. Zhang, H. Z. Yang, J. Y. Fang, S. Z. Zou, *Nano Lett.* **2010**, *10*, 638; l) Y. Kim, J. W. Hong, Y. W. Lee, M. Kim, D. Kim, W. S. Yun, S. W. Han, *Angew. Chem.* **2010**, *122*, 10395; *Angew. Chem. Int. Ed.* **2010**, *49*, 10197; m) A. X. Yin, X. Q. Min, Y. W. Zhang, C. H. Yan, *J. Am. Chem. Soc.* **2011**, *133*, 3816.

[12] S. Koh, P. Strasser, *J. Am. Chem. Soc.* **2007**, *129*, 12624.

[13] M. H. Shao, K. Shoemaker, A. Peles, K. Kaneko, L. Protsailo, *J. Am. Chem. Soc.* **2010**, *132*, 9253.

[14] P. Strasser, S. Koh, T. Anniyev, J. Greeley, K. More, C. F. Yu, Z. C. Liu, S. Kaya, D. Nordlund, H. Ogasawara, M. F. Toney, A. Nilsson, *Nat. Chem.* **2010**, *2*, 454.

[15] Y. H. Chen, H. H. Hung, M. H. Huang, *J. Am. Chem. Soc.* **2009**, *131*, 9114.

[16] a) M. H. Shao, T. Yu, J. H. Odell, M. S. Jin, Y. N. Xia, *Chem. Commun.* **2011**, *47*, 6566; b) M. Crespo-Quesada, J.-M. Andanson, A. Yarulin, B. Lim, Y. N. Xia, L. Kiwi-Minsker, *Langmuir* **2011**, *27*, 7909.

Received: August 24, 2011
Revised: November 9, 2011
Published online: December 13, 2011

